

A Physics-Based Circuit Model for Magnetic Tunnel Junctions

Steven Louis^{1*}, Hannah Bradley², Artem Litvinenko³, and Vasyl Tyberkevych²¹*Department of Electrical and Computer Engineering, Oakland University, Rochester, MI, 48309, USA*²*Department of Physics, Oakland University, Rochester, MI, 48309, USA*³*Department of Physics, University of Gothenburg, Fysikgränd 3, Gothenburg, 412 96, Sweden*

Abstract—This work presents an equivalent circuit model for Magnetic Tunnel Junctions (MTJs) that accurately captures their magnetization dynamics and electrical behavior. Implemented in LTspice, the model is validated against direct numerical solutions of the Landau-Lifshitz-Gilbert-Slonczewski (LLGS) equation. It effectively simulates essential spintronic phenomena, including ferromagnetic resonance, field- and spin-torque-induced switching, and spin-torque-induced oscillations. Simulation results demonstrate strong agreement between LTspice and LLGS solutions, confirming the model accuracy and utility for efficient circuit-level analysis of spintronic devices. The ability to incorporate time-dependent magnetic fields and voltage inputs makes the proposed model suitable for diverse applications such as neuromorphic computing, microwave signal processing, and spintronic memory technologies. By providing a computationally efficient yet physically accurate circuit representation, this work enables seamless integration of MTJs into larger electronic systems, potentially accelerating the development of advanced spintronic circuit architectures.

Index Terms— Magnetic tunnel junction (MTJ), equivalent circuit modeling, spin-transfer torque, spintronics, magnetoresistive random-access memory (MRAM), LTspice, circuit simulation, ferromagnetic resonance (FMR).

I. INTRODUCTION

In the past two decades, magnetic tunnel junctions (MTJs) revolutionized data storage by enabling high-density recording in disk-based drives [Chappert, 2007]. Beyond storage, MTJs integrated with CMOS technology have been commercially deployed in magnetoresistive random-access memory (MRAM) [Alzate 2015, Edelstein 2020], which utilizes non-volatility and fast switching properties of MTJs to provide energy-efficient and high-speed memory [Ikegawa 2020, Ikegawa 2021]. Beyond digital applications, MTJs can also be used as current-driven microwave sources [Fuchs 2004, Villard 2009], microwave detectors [Tulapurkar 2005], energy harvesters [Fang 2019] and more advanced microwave signal processing devices [Litvinenko 2022]. Recently, MTJs have also been explored neuromorphic computing applications [Romera 2018, Louis 2024, Rodrigues 2023].

An MTJ consists of two ferromagnetic layers separated by a thin insulating barrier [Singh 2019, Yuasa 2007]. The operational principle of an MTJ is based on the tunneling magnetoresistance effect, which is sensitive to the relative orientation of magnetic moments in the ferromagnetic layers [Yuasa 2007], and on the spin-transfer-torque (STT) effect [Slonczewski 1989, Ralph 2008] that describes influence of electric current on magnetization dynamics. Advanced nanoscale fabrication methods have enabled integration of MTJs into complex electronic systems, expanding their use in memory and logic devices [Alzate 2015, Edelstein 2020]. These distinctive properties position MTJs as important components in next-generation memory, analog, and neuromorphic computing systems [Incorvia 2024].

Circuit simulation is essential in the design and analysis of electronic systems [Najm 2010]. An accurate circuit-equivalent model of an MTJ facilitates its integration into larger circuits and allows comprehensive performance evaluation. Several MTJ circuit models have been previously proposed [Xu 2012, Panagopoulos 2012, Kim 2015], but they are based on formal mathematical equivalence of magnetization and circuit equations and do not faithfully represent physical aspects of MTJ behavior. For example, they do not contain energy storing elements (capacitance or inductance) that represent magnetic energy of an MTJ, or resistive elements describing Gilbert damping mechanism.

This letter introduces an equivalent circuit model for MTJs that accurately reflects their underlying physical characteristics. Within the proposed model, conservative magnetic interactions (e.g., effect of a bias magnetic field or magnetic anisotropy) are modeled by equivalent nonlinear capacitance and inductance. Dissipative magnetic torques are represented by equivalent resistance (Gilbert damping) and current and voltage sources (STT). The model is realized as a standalone element in LTspice electrical engineering software and its validity is demonstrated by comparing LTspice simulation results with direct numerical simulations of the Landau-Lifshitz-Gilbert-Slonczewski (LLGS) equation.

II. Physics-Based Equivalent MTJ Circuit

An MTJ comprises a ferromagnetic fixed layer, a non-magnetic spacer, and a ferromagnetic free layer, as shown in Fig. 1(a). The magnetization of the fixed layer is represented by \mathbf{p} , while the free layer magnetization is denoted by \mathbf{m} . The term “free layer” indicates that the magnetization direction can be altered by external stimuli, such as an applied magnetic field \mathbf{B}_{ext} or electric current I . In contrast, the fixed layer has a stable magnetization direction that

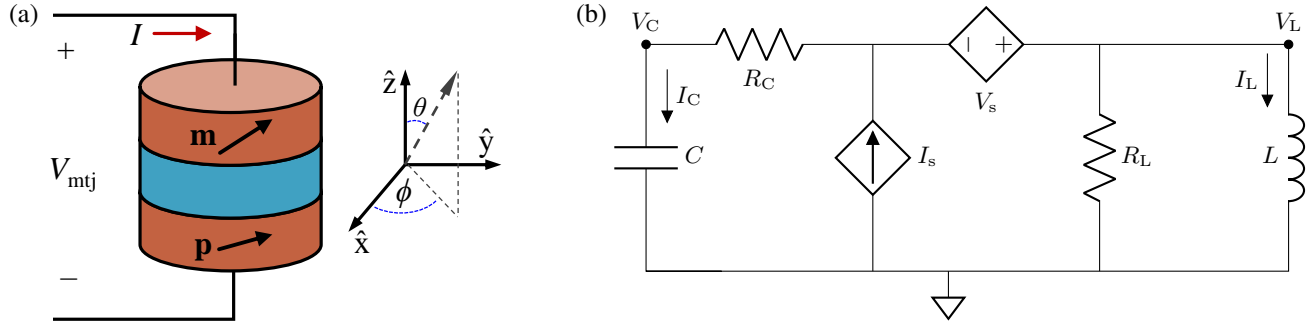


Fig. 1. (a) Schematic of the MTJ, illustrating the fixed and free layers. (b) Equivalent circuit representation of the MTJ free layer.

remains largely unaffected by external perturbations. The dynamic behavior of the free layer arises from the interplay between magnetic fields, damping effects, and spin-transfer torque, producing complex magnetization dynamics. These dynamics determine the electrical behavior and switching characteristics of MTJ-based devices [Slavin 2009].

When an electric current I passes through the MTJ, it encounters a resistance denoted as R_{mtj} . The resistance R_{mtj} reaches a minimum value, R_P , when the magnetization vectors \mathbf{p} and \mathbf{m} are parallel. Conversely, the resistance is maximized, taking the value R_{AP} , when \mathbf{p} and \mathbf{m} are antiparallel. If the vectors \mathbf{p} and \mathbf{m} are orthogonal, the resistance becomes R_{\perp} , defined by $R_{\perp} = 2R_{AP}R_P/(R_{AP} + R_P)$. A general expression for the resistance of an MTJ is provided by [Slonczewski 1989, Wang 2009],

$$R_{\text{mtj}} = \frac{R_{\perp}}{1 + \eta^2(\mathbf{p} \cdot \mathbf{m})}, \quad (1)$$

where η is the dimensionless spin polarization efficiency, given by $\eta = \sqrt{(R_{AP} - R_P)/(R_{AP} + R_P)}$.

The magnetization dynamics of the free layer can be effectively described using the macrospin approximation, which is governed by the Landau-Lifshitz-Gilbert-Slonczewski (LLGS) equation [Slavin 2009], given by

$$\frac{d\mathbf{m}}{dt} - |\gamma|\mathbf{B}_{\text{eff}} \times \mathbf{m} = \alpha_G \mathbf{m} \times \frac{d\mathbf{m}}{dt} - \mathbf{m} \times \mathbf{J}_s \times \mathbf{m}, \quad (2)$$

where γ is the gyromagnetic ratio, and α_G is the Gilbert damping parameter. The spin current \mathbf{J}_s can be written as $\mathbf{J}_s = (\gamma\hbar\eta/2eM_sV_s)(V_{\text{mtj}}/R_{\perp})\mathbf{p}$, where \hbar is the reduced Planck constant, μ_0 is the vacuum magnetic permeability, e is the elementary charge, V_s represents the volume of the free layer, and V_{mtj} is the voltage across the MTJ. The effective magnetic field \mathbf{B}_{eff} is given by $\mathbf{B}_{\text{eff}} = -(1/M_sV_s)\partial E(\mathbf{m})/\partial\mathbf{m}$, where $E(\mathbf{m})$ is the macrospin energy which is given by

$$E(\mathbf{m}) = M_sV_s \left[-B_e \cdot \mathbf{m} + \frac{1}{2}B_d(\mathbf{m} \cdot \hat{\mathbf{z}})^2 - \frac{1}{2}B_a(\mathbf{m} \cdot \hat{\mathbf{x}})^2 \right], \quad (3)$$

where B_e is the externally applied field, B_a is the easy-axis anisotropy field in the MTJ plane, and B_d is the effective demagnetizing field having contributions from dipolar field and perpendicular magnetic anisotropy (PMA).

As discussed above, Eq. (2) describes the free layer magnetization dynamics. Since MTJ resistance, R_{mtj} , depends on the relative

orientation of magnetization vectors, variations in \mathbf{m} directly affect device electrical behavior. In Eq. (2), the left side represents conservative precessional motion. On the right side, the first term describes Gilbert damping torque, and the second represents Slonczewski spin-transfer torque.

The macrospin model Eq. (2) can be represented by an equivalent nonlinear LC circuit by defining effective capacitor charge Q and inductor flux Φ as

$$Q = \frac{e}{\hbar} \frac{M_s V_{ot}}{\gamma} \cos \theta, \quad \Phi = \frac{\hbar}{e} \phi, \quad (4)$$

where θ and ϕ are, respectively, the polar and azimuthal angles of the magnetization vector \mathbf{m} (see Fig. 1(a)). For detailed derivation of the model see [Louis 2025].

Figure 1(b) presents the equivalent circuit LC model with additional elements that capture all aspects of the dynamics of the free MTJ layer. In this representation, the capacitor C and inductor L correspond to the conservative precessional dynamics terms in the LLGS equation. The resistors R_C and R_L model the dissipation associated with the Gilbert damping mechanism. The current source I_s and the voltage source V_s arise from Slonczewski spin-transfer torque.

Following standard definitions for electrical circuits, the current through the capacitor I_C and the voltage at the inductor V_L are defined as

$$I_C = \frac{\partial Q}{\partial t}, \quad V_L = \frac{\partial \Phi}{\partial t}. \quad (5)$$

Likewise, the voltage at the capacitor V_C and the current through the inductor I_L are related to the energy E of the LC circuit by

$$V_C = \frac{\partial E}{\partial Q}, \quad I_L = \frac{\partial E}{\partial \Phi}. \quad (6)$$

For an MTJ with energy function Eq. (3), these definitions give

$$V_C = \frac{\gamma\hbar}{e} \left[B_{e,z} - \frac{(B_{e,x} \cos \phi + B_{e,y} \sin \phi)}{\tan \theta} - (B_d + B_a \cos^2 \phi) \cos \theta \right], \quad (7)$$

$$I_L = \frac{\gamma\hbar}{eZ_s} \left[(B_{e,x} \sin \phi - B_{e,y} \cos \phi) \sin \theta + \frac{1}{2}B_a \sin(2\phi) \sin^2 \theta \right]. \quad (8)$$

Here, $Z_s = \hbar^2\gamma/(eM_sV_s)$ is a ‘‘characteristic impedance’’ of the macrospin – a quantity with dimension of electrical resistance that naturally appears in the equivalent circuit model.

These equations represent constitutive relations for equivalent macrospin capacitance and inductance and can be directly incorporated into modern electrical engineering software (e.g., LTspice) using various behavioral elements.

Other parameters of the equivalent circuit Fig. 1(b) are:

$$R_C = \frac{\alpha_G Z_s}{\sin^2 \theta}, \quad (9)$$

$$R_L = \frac{Z_s}{\alpha_G \sin^2 \theta}, \quad (10)$$

$$I_s = \frac{\eta}{2} \left[p_z \sin \theta - (p_x \cos \phi + p_y \sin \phi) \right] \sin \theta \frac{V_{\text{mtj}}}{R_{\perp}}, \quad (11)$$

$$V_s = \frac{\eta}{2} \left[\frac{p_x \sin \phi - p_y \cos \phi}{\sin \theta} \right] \frac{V_{\text{mtj}}}{R_{\perp}} Z_s. \quad (12)$$

For a complete derivation of the equivalent circuit model see [Louis 2025].

III. Validation of Equivalent Circuit Model

The circuit shown in Fig. 1(b) was implemented in LTspice, a widely used free simulation tool available at [Analog Devices]. This model simulates MTJ dynamics under time-dependent voltages V_{MTJ} and magnetic fields B_e . This section presents simulations of ferromagnetic resonance (FMR), operation of the MTJ as a spin-torque nano-oscillator (STNO), field-induced switching, and spin-torque switching. The LTspice model and all simulation files are available at [MTJ Spice Models].

A. Ferromagnetic Resonance

The FMR response was evaluated by comparing LTspice simulations of the equivalent circuit model with theoretical predictions. The simulations modeled free decay of magnetization oscillations, i.e., the magnetization was initialized slightly off equilibrium and then relaxed with oscillations at the FMR frequency. Simulations used a free layer with magnetization $M_s = 796$ kA/m ($B_d = \mu_0 M_s = 1$ T), volume of $V_s = 5.65 \times 10^{-24}$ m³, corresponding to an elliptical geometry of the free layer with a semi-axes of 30 nm and 20 nm and a thickness of 3 nm, and the anisotropy field $B_a = 0.2$ T. To precisely measure the FMR frequency, the Gilbert damping parameter was set to a small value of $\alpha_G = 0.0001$.

Figure 2(a) shows that LTspice simulations (red dots) and theoretical FMR frequencies $f_{\text{FMR}} = (\gamma/2\pi) \sqrt{(B_{e,x} + B_a)(B_{e,x} + B_a + B_d)}$ (black curve) closely match for fields applied along the easy axis (\hat{x} direction). The relative error is below 0.003% for all points.

Figure 2(b) presents simulation results for fields applied along the intermediate (\hat{y}) axis. For $B_{e,y} < B_a$, the theoretical FMR frequency is given by $f_{\text{FMR}} = (\gamma/2\pi) \sqrt{(B_{e,y} - B_a)(B_{e,y} + B_d)}$, and for $B_{e,y} > B_a$, it is equal to $f_{\text{FMR}} = (\gamma/2\pi) \sqrt{(B_a^2 - B_{e,y}^2)(B_a + B_d)/B_a}$. The circuit model accurately reproduces the mode transition at $B_{e,y} = B_a = 0.2$ T, with relative errors below 0.02% for all data points.

Similar results were also obtained for an applied field along the hard-axis (\hat{z}), with a relative error below 0.0025% for all points.

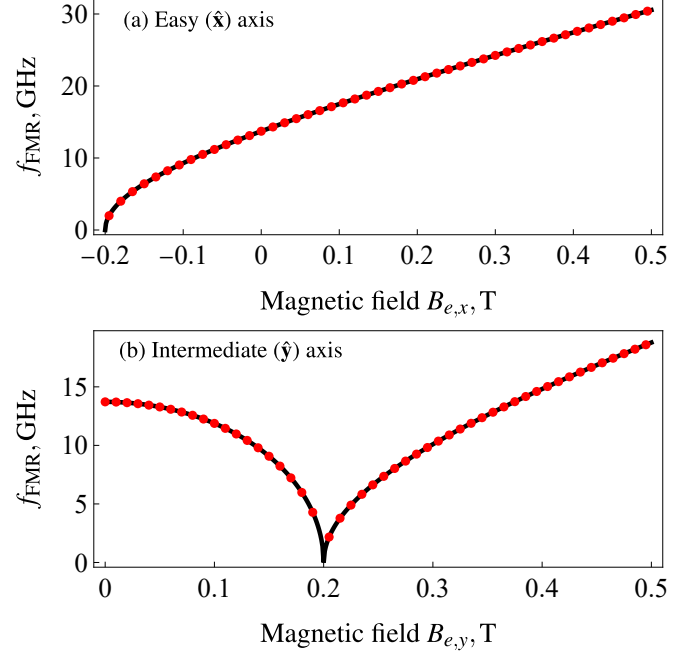


Fig. 2. Comparison of simulated and theoretical FMR frequencies as functions of applied magnetic fields. The red dots represent LTspice simulations, while the black curves correspond to analytical predictions derived from the LLGS equation. External magnetic field is applied along (a) the easy axis \hat{x} and (b) the intermediate axis \hat{y} .

The agreement between simulated FMR frequencies and theoretical values confirms the accuracy of the equivalent circuit. The extremely low error values demonstrate the validity of the circuit model for external magnetic fields oriented along the \hat{x} , \hat{y} , and \hat{z} axes, including cases involving anisotropy and mode transitions (e.g., when $B_{e,y} = B_a$).

B. Spin-Torque Nano-Oscillator

STNOs are nanoscale devices that use spin-transfer torque to generate self-sustained oscillations in the free layer magnetization, which produce a time-varying resistance in the MTJ [Slavin 2009]. Here, we demonstrate that the equivalent circuit model accurately reproduces large-amplitude oscillations in a current-driven MTJ.

Figure 3(a) shows the trajectory of the free layer magnetization, \mathbf{m} , simulated in LTspice with a spin-polarized current of 0.33 mA, $R_P = 500 \Omega$, $R_{AP} = 1500 \Omega$, spin polarization vector oriented at $\theta_p = 85^\circ$ and $\phi_p = 190^\circ$, Gilbert damping constant $\alpha_G = 0.01$, anisotropy field of $B_a = 0.2$ T, and external magnetic field components $B_{e,x} = -0.1$ T, $B_{e,y} = -0.15$ T, and $B_{e,z} = 0.8$ T. The free layer magnetization undergoes sustained precessional motion at approximately 14 GHz, characteristic of STNO operation. The trajectory has non-elliptical shape due to the combined effects of the effective field and spin-transfer torque.

Figures 3(b) presents the time evolution of the polar angle, θ and demonstrates that LTspice model produces results identical to LLGS equation. This close agreement demonstrates that the equivalent circuit accurately models all three components of the

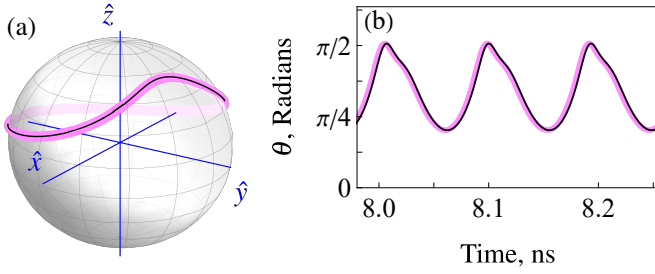


Fig. 3. Comparison of STNO dynamics obtained from LTspice and direct simulation of the LLGS equation. (a) Simulated trajectory of the free layer magnetization under a 0.33 mA applied current. (b) Time evolution of the polar angle θ . Black curves correspond to direct numerical simulation of the LLGS equation, while pink curves represent LTspice simulations.

LLGS equation: the conservative precession term, the damping term, and the spin-transfer anti-damping torque. The simulations specifically employed unconventional external magnetic fields and polarization angles designed to produce non-uniform and non-elliptical precession; despite this complexity, the equivalent circuit performed well. These results may find application in integrated STNO-based systems [Litvinenko 2022], where accurate circuit-level simulation of complex magnetization dynamics would be a valuable tool for designing complete circuit implementations.

C. Field-Induced Switching

In Fig. 4(a) we compare LTspice and LLGS simulations for field-induced switching of an MTJ. In this simulation, the system was subjected to a time-varying external magnetic field applied for 0.058 ns at intervals of 1.0 ns, with the field turned off otherwise. When active, the field had an amplitude of 0.4 T and was oriented in the xy plane at an angle 15° (green shading in Fig. 4(a)) or 195° (blue shading) to MTJ easy axis \hat{x} . Other simulation parameters are $R_P = 500 \Omega$, $R_{AP} = 1500 \Omega$, the anisotropy field of $B_a = 0.1$ T, Gilbert damping coefficient of $\alpha_G = 0.05$.

The strong agreement between LTspice and LLGS results, including accurate description of post-switching “ringing”, confirms the accuracy of the equivalent circuit model for large-angle (180°) magnetization rotation.

The previous two subsections demonstrated that the equivalent circuit functions accurately in stationary regimes, where magnetic fields and currents remain static while the output dynamically evolves. This section has shown that the circuit also performs reliably under time-varying magnetic fields. The example of field-induced switching was selected for its familiarity to the MRAM community, but additional tests (not shown) included a variety of time-dependent fields, such as sinusoidal and nonlinear impulses. In every case, the circuit produced results that closely matched macrospin simulations. Moreover, these simulations were straightforward to configure and fast to execute using the equivalent circuit in LTspice.

D. Current-Induced Switching in a 1T-1MTJ Cell

To further validate the equivalent circuit model and demonstrate the utility of LTspice simulations, the MTJ was integrated as a single LTspice component, available at [MTJ Spice Models 2025]. This integrated MTJ is highlighted by a yellow box in Figure 4(b), which shows a schematic of a 1T-1MTJ memory cell implemented in LTspice. A 1T-1MTJ cell consists of a single transistor and an MTJ connected in series, forming a compact unit suitable for high-density memory arrays [Guo 2015]. In this configuration, the wordline activates the write operation, while the bitline and source line provide the necessary bias and read voltages for proper cell operation. Current-induced switching occurs when an electric current reverses the magnetization of the free layer, toggling the MTJ between its low- and high-resistance states.

To evaluate the accuracy of the equivalent circuit model, current-induced switching was simulated in the 1T-1MTJ cell and compared to direct numerical simulation of the LLGS equation (see Fig. 4(c)). The excellent agreement between the two approaches confirms that the circuit model accurately reproduces the dynamics of current-induced switching.

In these simulations, a 5 V square wave with a period of 2 ns was applied alternately to the bitline and source line; the sourceline was at 5 V from 0 to 1 ns, and the bitline was at 5 V from 1 to 2 ns. Additionally, a 5 V square impulse lasting 0.1 ns was applied to the wordline at times 0.5 ns, 1.5 ns, and 2.5 ns. These applied voltage waveforms resulted in MTJ currents of approximately 10 mA at 0.5 ns and 2.5 ns (green shading in Fig. 4(c)) and -10 mA at 1.5 ns (blue shading). The spin polarization vector \mathbf{p} was oriented in the xy plane at 15° relative to the \hat{x} axis. Other simulation parameters were the same as in the field switching example.

This section demonstrates the potential of the equivalent circuit model for simulating hybrid circuits with MTJs and conventional electronic components. Although a relatively simple 1T-1MTJ cell was chosen for the example, the equivalent circuit is applicable to circuits of any complexity. The equivalent circuit has been integrated into a single LTspice part, and readers are invited to download and incorporate this part into their own simulations.

IV. Conclusion

In this work, we presented a physics-based equivalent circuit model for MTJs that accurately describes both magnetization dynamics and electrical characteristics. The proposed model was validated against direct numerical solutions of the LLGS equation across multiple operating regimes, including FMR, STNO, field- and current-induced switching. LTspice simulations demonstrated excellent agreement with numerical results, confirming the robustness and fidelity of the model.

All components of the equivalent circuit have a clear physical origin, and, as a result, the proposed model can be easily modified to describe more complicated spintronic devices, such as, e.g., MTJs with multiple free or fixed layers.

This work bridges spintronic physics and circuit-level implementation, providing an effective and efficient tool for the analysis and

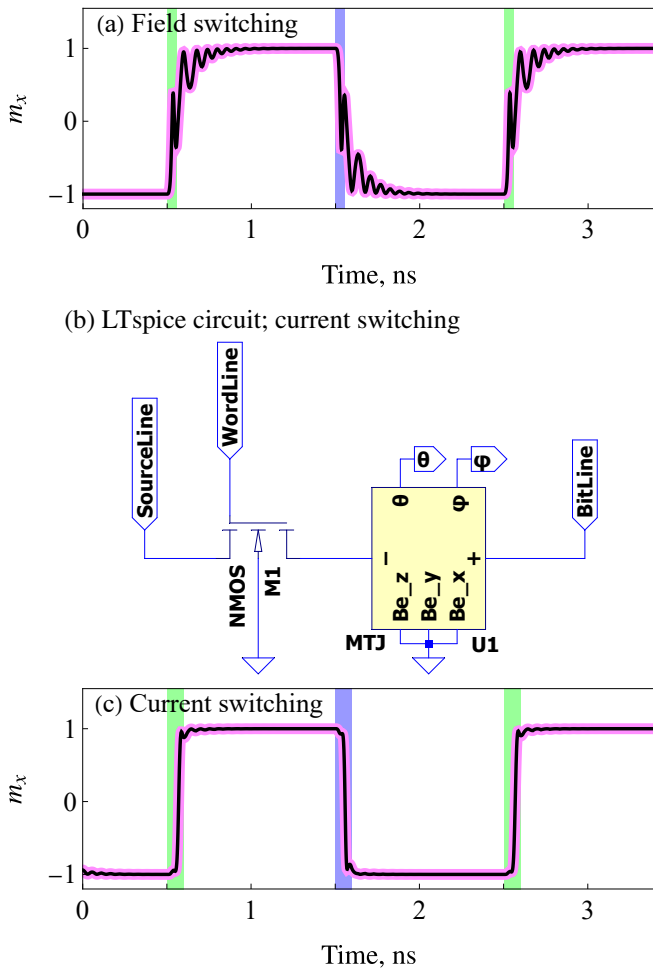


Fig. 4. (a) Field-induced switching dynamics. (b) Schematic of a 1T-1MTJ cell in LTspice, with the MTJ component highlighted by a yellow box. (c) Current-induced switching dynamics in a 1T-1MTJ cell. In (a) and (c), pink curves show LTspice simulations while black lines are results of direct numerical simulation of the LLGS equation.

design of spintronic devices. The results presented here support the development of next-generation non-volatile memory and advanced computing technologies based on spintronic elements.

REFERENCES

Alzate, J. G., Amiri, P. K., Wang, K. L. (2015). Magnetic tunnel junctions and their applications in non-volatile circuits. In Handbook of Spintronics (pp. 1127-1171). Springer Netherlands.

Edelstein, D., Rizzolo, M., Sil, D., Dutta, A., DeBrosse, J., Wordeman, M., ... Worledge, D. C. (2020, December). A 14 nm embedded STT-MRAM CMOS technology. In 2020 IEEE International Electron Devices Meeting (IEDM) (pp. 11-5). IEEE.

Ikegawa S, Mancoff FB, Janesky J, Aggarwal S. Magnetoresistive random access memory: Present and future. (2020). IEEE Transactions on Electron Devices. Jan 30;67(4):1407-19.

Ikegawa S, Mancoff FB, Aggarwal S. Commercialization of mram—historical and future perspective. (2021). In2021 IEEE International Interconnect Technology Conference (IITC) Jul 6 (pp. 1-3). IEEE.

Fuchs, G. D., N. C. Emley, I. N. Krivorotov, P. M. Braganca, E. M. Ryan, S. I. Kiselev, J. C. Sankey, D. C. Ralph, R. A. Buhrman, and J. A. Katine. (2004). Spin-transfer effects in nanoscale magnetic tunnel junctions. Applied Physics Letters 85, no. 7: 1205-1207.

Villard, P., Ebels, U., Houssameddine, D., Katine, J., Mauri, D., Delaet, B., Vincent, P., Cyrille, M.C., Viala, B., Michel, J.P. and Prouvee, J. (2009). A GHz spintronic-based RF oscillator. IEEE Journal of solid-state circuits, 45(1), pp.214-223.

Tulapurkar, A. A., Y. Suzuki, A. Fukushima, H. Kubota, H. Maehara, K. Tsunekawa, D. D. Djayaprawira, N. Watanabe, and S. Yuasa. (2005). Spin-torque diode effect in magnetic tunnel junctions. Nature 438, no. 7066 (2005): 339-342.

Litvinenko, Artem, Ahmed Sidi El Valli, Vadym Iurchuk, Steven Louis, Vasyl Tyberkevych, Bernard Diény, Andrei N. Slavin, and Ursula Ebels. (2022). Ultrafast GHz-range swept-tuned spectrum analyzer with 20 ns temporal resolution based on a spin-torque nano-oscillator with a uniformly magnetized “free” layer. Nano Letters 22, no. 5: 1874-1879.

Romera, M., Talatchian, P., Tsunegi, S., Abreu Araujo, F., Cros, V., Bortolotti, P., Trastoy, J., Yakushiji, K., Fukushima, A., Kubota, H. and Yuasa, S. (2018). Vowel recognition with four coupled spin-torque nano-oscillators. Nature, 563(7730), pp.230-234.

Fang, B., Carpentieri, M., Louis, S., Tiberkevich, V., Slavin, A., Krivorotov, I.N., Tomasello, R., Giordano, A., Jiang, H., Cai, J. and Fan, Y. (2019). Experimental demonstration of spintronic broadband microwave detectors and their capability for powering nanodevices. Physical Review Applied, 11(1), p.014022.

Louis, S., Bradley, H., Trevillian, C., Slavin, A. and Tyberkevych, V. (2024). Spintronic Neuron Using a Magnetic Tunnel Junction for Low-Power Neuromorphic Computing. IEEE Magnetics Letters. IEEE.

Rodriguez D R, Moukhaider R, Luo Y, Fang B, Pontlevy A, Hamadeh A, Zeng Z, Carpentieri M, Finocchio G (2023). Spintronic Hodgkin-Huxley-analogue neuron implemented with a single magnetic tunnel junction. Phys. Rev. Appl., vol. 19, 064010, doi: 10.1103/PhysRevApplied.19.064010.

Singh, J.P., Bhardwaj, R., Sharma, A., Kaur, B., Won, S.O., Gautam, S. and Chae, K.H. (2019). Fabrication of magnetic tunnel junctions. In Advanced Applications in Manufacturing Engineering (pp. 53-77). Woodhead Publishing.

Yuasa, S. and Djayaprawira, D.D., (2007). Giant tunnel magnetoresistance in magnetic tunnel junctions with a crystalline MgO (0 0 1) barrier. Journal of Physics D: Applied Physics, 40(21), p.R337. APS.

Slonczewski, J.C., (1989). Conductance and exchange coupling of two ferromagnets separated by a tunneling barrier. Physical Review B, 39(10), p.6995.

Ralph, D.C. and Stiles, M.D. (2008). Spin transfer torques. Journal of Magnetism and Magnetic Materials, 320(7), pp.1190-1216.

Tehrani, S., Engel, B., Slaughter, J.M., Chen, E., DeHerrera, M., Durlam, M., Naji, P., Whig, R., Janesky, J. and Calder, J., (2000). Recent developments in magnetic tunnel junction MRAM. IEEE Transactions on magnetics, 36(5), pp.2752-2757. IEEE.

Gallagher, W.J. and Parkin, S.S., (2006). Development of the magnetic tunnel junction MRAM at IBM: From first junctions to a 16-Mb MRAM demonstrator chip. IBM Journal of Research and Development, 50(1), pp.5-23.

Incorvia, J.A.C., Xiao, T.P., Zogbi, N., Naeemi, A., Adelman, C., Catthoor, F., Tahoori, M., Casanova, F., Becherer, M., Prenat, G. and Couet, S., (2024). Spintronics for achieving system-level energy-efficient logic. Nature Reviews Electrical Engineering, pp.1-14. Nature.

Najm, F.N. (2010). Circuit simulation. John Wiley & Sons.

Xu, Z., Sutaria, K.B., Yang, C., Chakrabarti, C. and Cao, Y. (2013). Compact modeling of STT-MTJ for SPICE simulation. In 2013 Proceedings of the European Solid-State Device Research Conference (ESSDERC) (pp. 338-341). IEEE.

Panagopoulos, G.D., Augustine, C. and Roy, K. (2013). Physics-based SPICE-compatible compact model for simulating hybrid MTJ/CMOS circuits. IEEE Transactions on Electron Devices, 60(9), pp.2808-2814. IEEE

Kim, J., Chen, A., Behin-Aein, B., Kumar, S., Wang, J.P. and Kim, C.H. (2015). A technology-agnostic MTJ SPICE model with user-defined dimensions for STT-MRAM scalability studies. In 2015 IEEE custom integrated circuits conference (CICC) (pp. 1-4). IEEE.

Slavin, A. and Tiberkevich, V. (2009). Nonlinear auto-oscillator theory of microwave generation by spin-polarized current. IEEE Transactions on Magnetics, 45(4), pp.1875-1918.

Wang, C., Cui, Y.T., Sun, J.Z., Katine, J.A., Buhrman, R.A. and Ralph, D.C. (2009). Sensitivity of spin-torque diodes for frequency-tunable resonant microwave detection. Journal of Applied Physics, 106(5).

Analog Devices, Inc. (2024). LTspice—A high-performance SPICE simulator, schematic capture, and waveform viewer. Available at: <https://www.analog.com/en/resources/design-tools-and-calculators/ltspice-simulator.html> [Accessed March 14, 2025].

Guo, X. (2015). Energy-efficient architectures based on STT-MRAM. Ph.D. dissertation, University of Rochester.

MTJ Spice Models. Available at: <https://sites.google.com/view/mtjspicemodels/home> [Accessed March 25, 2025].

Louis, S., Bradley, H. and Tyberkevych, V. (2025). Equivalent Electric Model of a Macrospin. arXiv preprint arXiv:XXXX.XXXXX.